Available online at www.sciencedirect.com
SCIENCE DIRECT®
Journal of Solid State Chemistry 177 (2004) 1976–1986
JOURNAL OF SOLID STATE CHEMISTRY
http://elsevier.com/locate/jssc

The chromium tungsten nitride system: evidence of a disorder–order phase transformation

K.S. Weil*

Pacific Northwest National Laboratory, Department of Materials Science, Battelle Blvd., Richland, WA 99352, USA

Received 22 September 2003; received in revised form 19 January 2004; accepted 28 January 2004

Abstract

A detailed investigation of the synthesis of $CrWN_2$ from a chemical precursor has revealed that it forms via an intermediate disordered nitride. The kinetics of this disordered to ordered phase transformation have been determined and suggest that the layered compound nucleates and grows epitaxially out of the disordered nitride via a two-dimensional transformation mechanism in which cation ordering takes place at the interface between the two structures. Results from high-resolution transmission electron microscopy analysis were used to identify the interfacial relationship between the disordered and ordered phases. In combination with our kinetic data, this information implies that ordering occurs through a short-range, interfacially controlled diffusional process.

Published by Elsevier Inc.

Keywords: Transition metal nitridges, phase transformation

1. Introduction

$CrWN_2$ is one of a handful of known layered ternary transition metal nitrides, all of which fall into one of two structural categories: hexagonal (prototype: a-$NaFeO_2$) or trigonal (prototype: $LiMoN_2$) [1–5]. This particular compound crystallizes in the trigonal structure [6] with its constituent atoms distributed over the following Wyckoff positions in the *R*3 (146) space group, hexagonal axes: 1Cr in 3(*a*) at (0, 0, 0.8251(7)), 1W in 3(*a*) at (0,0,0), 1N in 3(*a*) at (0, 0, 0.2629(6)), and 1N in 3(*a*) at (0, 0, 0.4068(5)). The layering in $CrWN_2$ results from the stacking of alternating closest-packed sheets of tungsten, nitrogen, chromium, nitrogen, etc. along the *z*-axis, where each tungsten atom lies in trigonal prismatic coordination with six neighboring nitrogen atoms, three from the nitrogen layer above and three from below, and the chromium atoms sit within the octahedral interstices formed between the two adjacent nitrogen layers that lie on either side of the chromium layer. These polyhedral arrangements are represented in Fig. 1(a). The alternating layers of edge-sharing WN_6 trigonal prisms and edge-sharing CrN_6 octahedra are stacked in an AA′BB′CC′ manner along the *c*-axis, where A, B, and C are the WN_6 layers and A′, B′, and C′ are the CrN_6 layers, as shown in Fig. 1(b), thus defining a trigonal structure as opposed to the AA′BB′AA′BB′ stacking arrangement found in the hexagonal layered compounds.

An alternative means of visualizing the layered arrangement of $CrWN_2$, which is particularly useful when interpreting high-resolution microscopy data, is to recognize that the nitrogen layers on either side of any given tungsten layer are stacked in coincident pairs, with one adjacent nitrogen layer positioned directly over the other. As shown in Fig. 1(b), these paired nitrogen layers are stacked in $CrWN_2$ in an a–a–b–b–c–c⋯ arrangement in a manner similar to that seen in FCC stacking. From this perspective, the chromium layers 'dictate' the forward $+\frac{1}{3}$, $+\frac{1}{3}$ shift of the N–W–N slabs in the x, y plane as they are stacked along the *c*-axis.

Recently, Svensson and Weil [7] conducted lattice image studies on $CrWN_2$ by high-resolution transmission electron microscopy (HRTEM) and reported the observance of two distinctive types of structural defects in this layered compound: twinning and intergrowth phases. Twinning in $CrWN_2$ can be visualized as a

*Fax: +509-375-4448.
E-mail address: scott.weil@pnl.gov.

0022-4596/$ - see front matter Published by Elsevier Inc.
doi:10.1016/j.jssc.2004.01.023

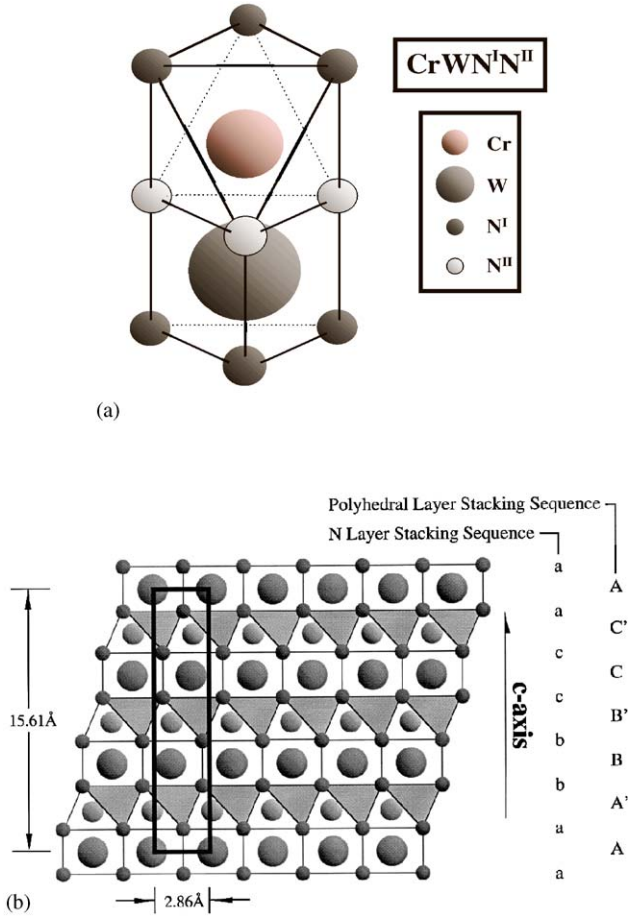

Fig. 1. Proposed structure for $CrWN_2$ displaying: (a) a polyhedral model of the trigonal prismatic coordination of nitrogen around tungsten and of the octahedral nitrogen coordination around chromium, and (b) the stacking sequence of the WN_6 trigonal prism layers and the CrN_6 octahedral layers, or alternatively the nitrogen layers, in $CrWN_2$. The tungsten atoms are denoted by the large dark gray spheres, chromium by the medium light gray spheres, and nitrogen by the small dark gray spheres. The unit cell of $CrWN_2$ is outlined by the heavy black lines.

mirror plane that runs midway inside and parallel to a trigonal prismatic layer. That is, the WN_6 trigonal prism layers can trigger a backward x, y shift $(-\frac{1}{3}, -\frac{1}{3})$ of an adjacent CrN_6 octahedral layer, causing the packing sequence along the c-axis to become a–a–b–b–c–c–a–|–a–c–c–b–b–a–a. Intergrowth defects also appeared frequently in the microstructure of this multicomponent nitride. HRTEM micrographs and corresponding image simulations of the intergrowth regions in $CrWN_2$ suggest that these defects are an epitaxially matched rock-salt structured phase. Unfortunately, high spatial microanalysis of the intergrowth regions was not available to determine the composition of the intergrowth phase, although there appeared to be enough contrast in the simulated images to allow the authors to speculate that the phase might be cubic chromium nitride, CrN. As will be presented below, there is very strong evidence for a disorder–order phase transformation in this system in which disordered, rock-salt structured chromium tungsten nitride, rs-$Cr_{0.5}W_{0.5}N$ transforms to the stable, layered chromium tungsten dinitride phase, L-$CrWN_2$. In light of this finding, the original HRTEM analysis will be revisited and an alternative explanation will be proposed that not only accounts for the presence of the intergrowth phase, but also offers a potential mechanism by which the phase transformation in this system may take place.

2. Experimental

2.1. Sample preparation

2.1.1. Precursor synthesis

All chemical manipulations were conducted in an argon-filled glovebox (O_2 and $H_2O \leqslant 5$ ppm) or under a protective stream of ultrahigh-purity nitrogen unless otherwise noted. All glassware used were acid washed with NoChromix and oven dried prior to use. Chromium (III) chloride hexahydrate (99.995%, Aldrich) and tungsten hexachloride (99.9+%, Aldrich) were dissolved in equal molar amounts in anhydrous acetonitrile (99.8%, Aldrich) forming a mixed complexed-metal solution of $CrCl_3 \cdot 2CH_3CN$ and $WOCl_2 \cdot 3CH_3CN$ [7,8]. The two ammonia adducted metal species were then precipitated simultaneously by slowly bubbling anhydrous ammonia (electronic grade, Matheson) through the solution, forming a dark blue colloid, which remained suspended in the acetonitrile phase. Evaporation of the acetonitrile yielded a dark blue powdery solid, which was further dried under vacuum at 90°C for 6 h. Used as the precursor for the chromium tungsten nitrides, this powder was analyzed and found to be essentially a finely divided mixture of two ammonia-complexed species, $[Cr(NH_3)_6]Cl_2$ and $WOCl_2 \cdot 3NH_3$ [8,9].

2.1.2. Heat treatment

The batches of precursor used in this study were all pre-treated at 600°C for 10 h in flowing ammonia (~130 mL/min). This was done to eliminate known impurities, such as ammonium chloride, to drive off the complexed ammonia groups, and to ammonolyze the chlorine and oxygen. X-ray diffraction (XRD; $\theta-\theta$ diffractometer, Rigaku Corporation), Fourier transform infrared spectroscopy (FTIR; Galaxy Series FTIR 5000, ATI Mattson), and quantitative chemical analyses confirmed that when pre-treated under the above conditions, the precursor will consistently form a stable, disordered rock-salt structured chromium tungsten nitride, rs-$Cr_{0.5}W_{0.5}N$ [8], which was used as the starting material for the phase transformation studies.

Isothermal heat treatment studies were conducted on rs-$Cr_{0.5}W_{0.5}N$ to investigate its transformation to the layered ternary nitride. Samples of the pre-treated powder weighing $\sim$0.5 g were placed in aluminum nitride crucibles measuring 20 mm × 40 mm × 5 mm tall, producing a powder bed depth of $\sim$2 mm. A horizontal tube furnace and $2\frac{1}{2}''$ diameter quartz tube were employed in these experiments. The back end of the tube furnace was connected to a mineral oil bubbler and the front end was connected to the ammonia gas line via borosilicate end caps to isolate the sample from ambient atmosphere during heat treatment. Prior to initiating the heat treatment, the tube was purged for 20 min with pre-pure nitrogen, then purged an additional 10 min with the heat treatment gas, 120 mL/min flowing ammonia. The phase transformation experiments were conducted by positioning the crucible inside the quartz tube such that it sat just outside the hot zone of the furnace prior to the isothermal soak, allowing it to equilibrate with the heat treatment atmosphere at a temperature that was $\sim$150–200°C below the soak temperature. The quartz tube was then slid into the furnace far enough for the sample to sit in the center of the hot zone. Based on a blank run, the time required for the sample to thermally equilibrate was approximately 20–30 s. After the desired heat treatment time, the quartz tube was pushed back out of the furnace past its original position so that the sample could quench to a temperature below 600°C within 30 s. In order to prevent the equilibration or cooling times from becoming a significant fraction of the transformation time, the shortest soak time employed in these studies was limited to 6 min.

Attempts to conduct the transformation studies in dry nitrogen and dry helium always lead to the formation of a small amount of oxide impurities, whereas the ammonia atmosphere yielded pure nitrides. Preliminary calculations of the amount of rs-$Cr_{0.5}W_{0.5}N$ to L-$CrWN_2$ transformation in nitrogen for a given transformation temperature, neglecting the effect of the oxides, were compared with those for the analogous transformations in ammonia and were consistent within 4–7%. Based on these findings, ammonia was chosen as the heat treatment atmosphere for the entire phase transformation investigation.

2.2. Sample characterization

The initiation time for the rs-$Cr_{0.5}W_{0.5}N$ to L-$CrWN_2$ transformation was recorded at several different temperatures by heating $\sim$20 mg samples in platinum cups in a differential thermal analysis system (TA Instruments) at 5°C/min under flowing ammonia. The extent of transformation was measured by quantitative XRD using a Rigaku θ/θ diffractometer. Percentages of the rock-salt and layer structured phases were estimated from the diffractograms of each heat treated powder by a direct comparison technique in which the peaks of the layered phase act as an internal standard [10]. The average deviation in the percentage transformed was found to be $\sim$6 w/o, as estimated from a series of samples heat treated independently under identical conditions. Diffraction data for the rs-$Cr_{0.5}W_{0.5}N$ and L-$CrWN_2$ phases were refined using the Rietveld refinement program, FULLPROF [11]. The profile shape was represented by the modified pseudo-Voigt function [12], with profile asymmetry introduced by employing a multiterm Simpson's rule integration [13]. In addition to the profile, lattice, structure parameters, the zero-point shift, nine background parameters, the scale factor, and the chromium and tungsten stoichiometries were also refined. Atomic thermal displacements were assumed to be isotropic.

Quantitative chemical analyses were performed by Galbraith Laboratories (Knoxville, Tennessee) on selected samples to confirm chromium, tungsten, and nitrogen stoichiometry. Inductively coupled plasma optical emission spectroscopy was used to determine the concentration of the metal species; combustion analyses using Leco analysis equipment were employed to evaluate the nitrogen, carbon, and oxygen contents following the American Society for Testing and Materials standard ASTM D5373 [14], while coulometric titration was used to analyze for particularly low concentrations of these species; and ion chromatography and capillary electrophoresis techniques were used to determine the chlorine levels.

Several of the partially transformed samples were examined by transmission electron microscopy (TEM) to visually observe changes in the powders due to the transformation and to examine whether an orientation relationship exists at the interfaces between the two phases; information which could help identify the type of mechanism by which the transformation takes place. For these studies, a small amount of the nitride sample was ground in an agate mortar and mixed with *n*-butanol to form a slurry. The slurry was ultrasonicated for 10 min to break up agglomerates. The sample was then re-ground in *n*-butanol and sonicated for 3 more minutes, then allowed to settle for at least 2 more minutes. A drop of the supernatant liquid was placed onto a holey carbon film supported by a copper grid and the butanol was allowed to evaporate. Conventional electron diffraction studies and microanalysis of single-crystallite fragments were performed using a Philips EM 420 scanning TEM equipped with a PGT System 4 Plus energy dispersive X-ray analyzer and a Gatan PLEES. Results from the previous HRTEM analysis that will be re-examined below were produced using a JEOL JEM 3010 microscope with a top-entry double-tilt goniometer (1.7 Å point-to-point resolution) operating at 300 kV. HRTEM image simulations were prepared using the program suite Mac Tempas.

3. Results and discussion

3.1. Transformation kinetics

It was originally observed in a series of scoping experiments that the chromium–tungsten precursor does not transform directly to the layered dinitride, but does so via an intermediate nanocrystalline disordered, or alloyed, rock-salt structured nitride phase characterized by XRD and chemical analyses as $Cr_{0.5}W_{0.5}N$ [6]. To examine this transformation in greater detail, samples of the rs-$Cr_{0.5}W_{0.5}N$ powder were heated under flowing ammonia in the DTA to three separate temperatures, 650°C, 700°C, and 750°C, at 3°C/min and held isothermally for 80, 80, and 37.5 h, respectively. As seen by the broad, relatively shallow exotherms displayed in the DTA curves in Figs. 2(a)–(c), the disordered chromium tungsten nitride undergoes an isothermal solid-state transformation at each of these temperatures. At 650°C, the transformation initiates approximately 489 min into the isothermal hold, while the transformations at 700°C and 750°C begin more quickly, starting after 253 and 141 min, respectively. The kinetic details of the solid-state transformation were further elucidated by heat treating samples of the rs-$Cr_{0.5}W_{0.5}N$ material under a series of 36 different isothermal soak conditions, conducting XRD analyses on the resulting powders to determine the type and quantity of phases present, and analyzing the results as a function of time at the given temperature.

The theoretical basis for analyzing isothermal phase transformation kinetics was originally derived by Johnson and Mehl [15] and by Avrami [16]. JMA (Johnson, Mehl, and Avrami) theory can be applied to a wide variety of interface-reaction-controlled or diffusion-controlled transformations, making it particularly useful in abstracting detailed information about the nucleation and growth kinetics for a given phase transformation. For example, the following expression derived by JMA can be used to determine the amount of transformation that has taken place over a specified period of time at a given isothermal soak temperature:

$$f = 1 - \exp(-kt^n), \quad (1)$$

where f is the fraction transformed, k is the transformation rate constant, t is the time of the transformation, and n is a constant, defined below, related to the physical characteristics of the newly transformed phase [17]. The rate constant k is related to the activation energy for the transformation through the Arrhenius expression:

$$k = A \exp(-E_a/RT), \quad (2)$$

where A is a factor associated with the diffusion of atoms across the interface between the two phases, E_a is the activation energy for the transformation, R is the universal gas constant, and T is the absolute temperature.

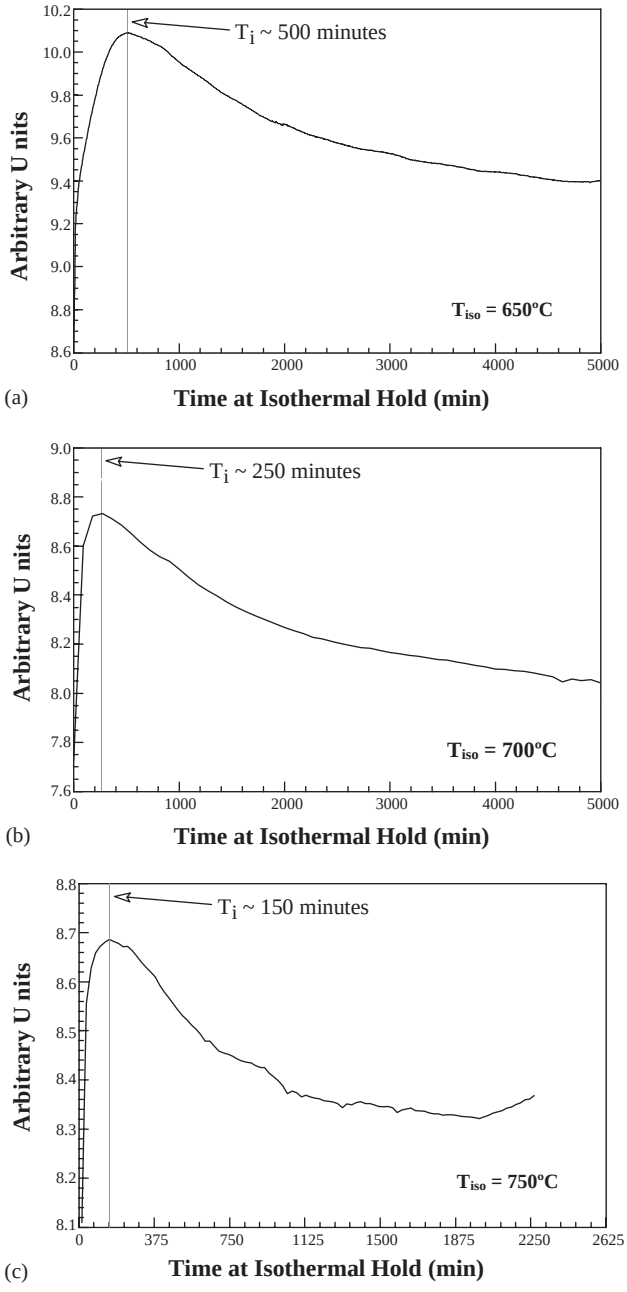

Fig. 2. DTA results displaying the exotherms associated with the solid-state transformations at: (a) 650°C, (b) 700°C, and (c) 750°C. Note the decrease in the incubation time, T_i, as the isothermal temperature is increased.

Based on the diffraction data collected on powders isothermally held at 600°C, 650°C, 675°C, 700°C, 750°C, and 775°C, a set of isothermal transformation curves was developed, as shown in Fig. 3. Incubation times for the onset of the transformation were determined by extrapolating the linear portion of the transformation curve to the time axis. The transformation from the disordered rock-salt phase to the layered

phase appears to follow JMA transformation kinetics. The S-shaped curves in this figure are not the result of a curve-fitting algorithm, but are drawn to represent a JMA-type transformation. The incubation time for the formation of the layered phase steadily decreases with increasing temperature. The nucleation rate for the layered phase is initially slow, regardless of the transformation temperature, as evidenced by the shallow slopes of the curves at low values of percent $CrWN_2$ transformed. As the layered phase nuclei begin to grow and achieve their maximum growth rate, approximately in the 5–10% transformed range, the slopes of the transformation curves increase dramatically. The curves finally plateau at ~90% transformed, as the growing L-$CrWN_2$ crystallites eventually impinge with each other and the bordering rs-$Cr_{0.5}W_{0.5}N$ phase is consumed.

Using the data shown in Fig. 3, a plot of $\ln[\ln(1-f)^{-1}]$ versus $\ln(t)$ was constructed to determine the rate constant and corresponding activation energy for the transformation, as shown in Fig. 4. Data not included in this analysis of transformation kinetics were those below 5% and those at 100% transformation to avoid significant errors arising from the estimation of induction time and final transformation time. Regression analysis was used to fit each set of data to a straight line. Note that the lines are approximately parallel, indicating that, within experimental error, the slopes are essentially equivalent. Employing the expression in Eq. (1) to describe the kinetics of the transformation, the slope of the lines in Fig. 4 represent the time exponent, n, which based on classical nucleation and growth theory is generally expected to be temperature independent. The average value of n given by this data is 1.04. On the other hand, the rate constants, k, are expected to increase with increasing temperature for a thermally activated process, which is indicated in Fig. 4 by the translation of the isothermal lines to the left. The values of k are determined from the y-intercepts in the regression equations representing these lines. Subsequently, by plotting the values of k against $1/T$, as shown in Fig. 5, the activation energy for the transformation reaction was determined using the Arrhenius expression in Eq. (2). The slope of the regression fitted line is E_a/R, from which the activation energy for this transformation was found to be $E_a = 126.4\,\mathrm{kJ/mol\,K}$. This value is on the same order,

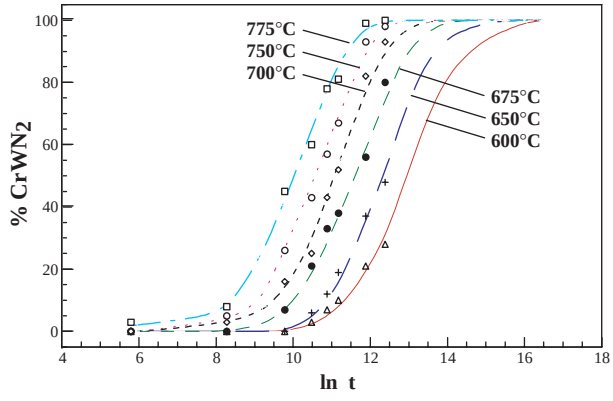

Fig. 3. Isothermal transformation curves for the chromium–tungsten precursor heat treated in anhydrous ammonia. Time, t, is in seconds.

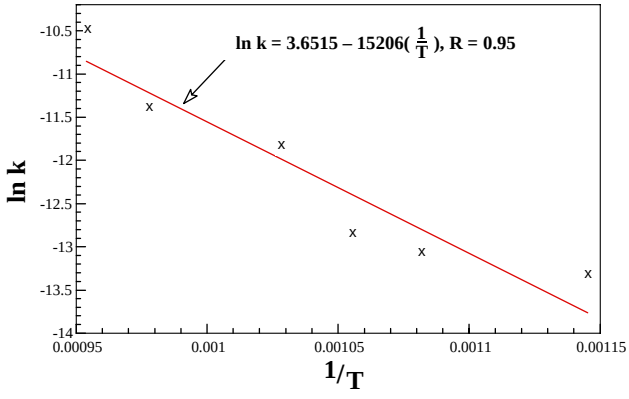

Fig. 5. A plot of $\ln k$ versus $1/T$ for the isothermally heat treated chromium–tungsten precursors given in Fig. 3.

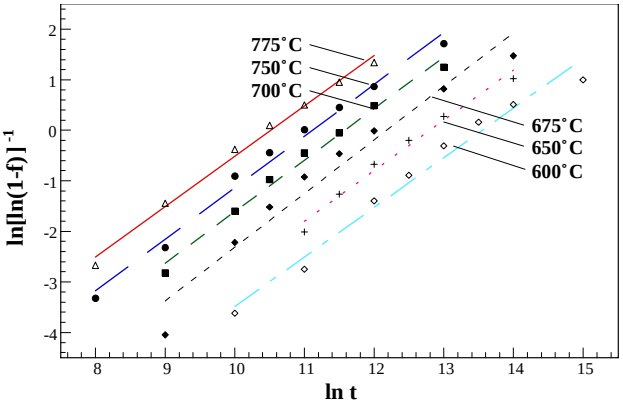

Fig. 4. A plot of $\ln[\ln(1-f)^{-1}]$ for the isothermally heat treated chromium–tungsten precursors given in Fig. 3. Time, t, is in seconds.

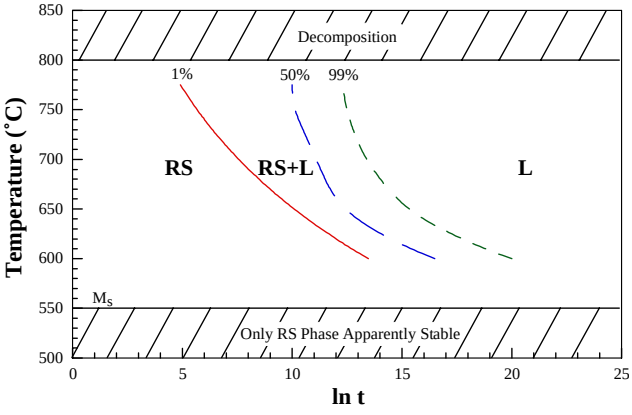

Fig. 6. A time–temperature–transformation plot for the Cr:W 1:1 nitride system.

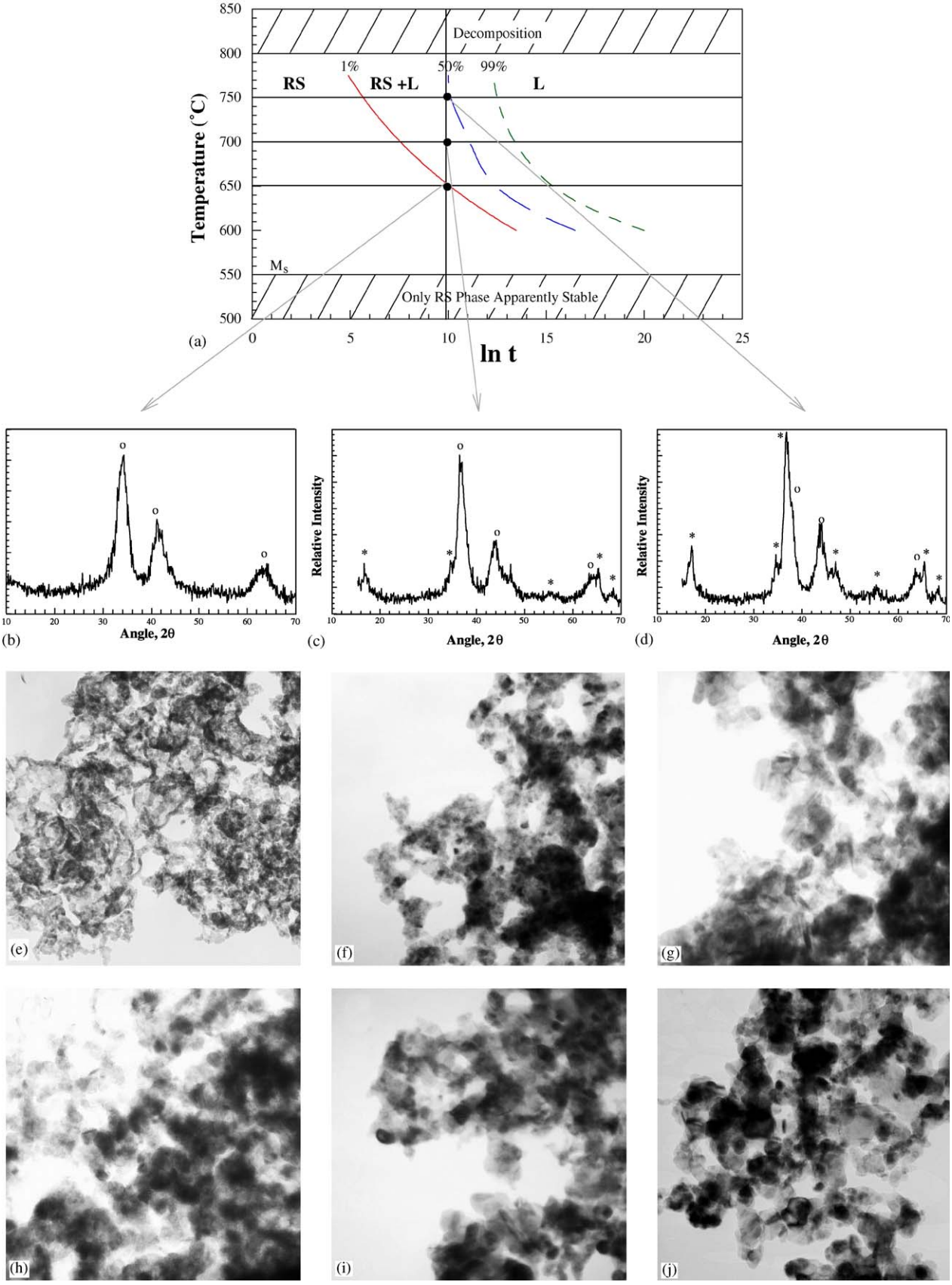
Decomposition
1%
50%
99%
RS
RS +L
L
Temperature (°C)
Ms
Only RS Phase Apparently Stable
ln t
(a)
Relative Intensity
Angle, 2θ
(b)
(c)
(d)
(e)
(f)
(g)
(h)
(i)
(j)

although in general smaller, as those reported for solid-state transformations in other ceramic systems, such as: 320 kJ/mol K for γ-Al_2O_3 to α-Al_2O_3 [18], 210 kJ/mol K for α''-$Fe_{16}N_2$ to γ'-$Fe_{16}N_2$ [19], and 500 kJ/mol K for α-Si_3N_4 to β-Si_3N_4 [20].

Based on the S-shaped transformation curves displayed in Fig. 3, a transformation–time–temperature (TTT) curve for this system was drawn, as shown in Fig. 6. Note that the traditional C-shape of the TTT curves is truncated because above 775°C the layered phase is not stable, but decomposes into Cr_3W_3N, CrN, and W_2N. On the other hand, a series of isothermal experiments conducted at 500°C and 550°C for $1\frac{1}{2}$ weeks showed no signs of the rock-salt to layered structure transformation, suggesting that the M_{start} temperature for this transformation lies at or above 550°C.

3.2. Transformation mechanism

Given the XRD results discussed above, which demonstrate a JMA-type transformation from the disordered rock-salt phase to the layered phase, TEM studies were initiated in an attempt to visually observe changes in the powders due to the transformation. As shown in Figs. 7 and 8, two sets of TEM analyses were conducted: (1) examining samples which were heat treated at three different temperatures, 650°C, 700°C, and 750°C, for the same amount of time, 5 h, and (2) examining samples which were held isothermally at 700°C for three different soak times, 6 min, 5, and 70 h. These figures give an account of these soak conditions, the resulting XRD patterns, and the morphologies and microstructures of the nitride powders.

Evident from the changes in the relative intensities of the rock-salt phase peaks (o) and layered phase peaks (asterisks) in the XRD patterns of Figs. 7(b)–(d), when rs-$Cr_{0.5}W_{0.5}N$ is held isothermally for 5 h at correspondingly higher temperatures, the fraction of newly transformed layered phase in each sample increases. The morphology and microstructure also changes significantly with increasing heat treatment temperature, as shown in the low- and high-magnification micrograph sequences in Figs. 7(e)–(g) and (h)–(j). The 650°C nanocrystalline rock-salt structured powder is very rounded, almost spherical in shape, while the 750°C powder displays a faceted, platelet-like appearance, which is evident from the fringes in the corresponding micrographs. In fact, in several of the micrographs, notably Figs. 7(i) and (j), it appears that a number of the platelets assume a well-faceted hexagonal shape, indicating the presence of the layered phase. The spheroids are on the order of 10–20 nm in diameter, whereas the platelets have general width and thickness dimensions of approximately 10–20 and 1–2 nm, respectively. Local chemical analysis of the powders via energy dispersive X-ray analysis (EDAX) and parallel electron loss spectrometry (PEELS) confirmed the 1:1:2 ratio of chromium to tungsten to nitrogen in each case.

The time evolution sequence of XRD and microstructural data in Fig. 8 exhibit trends that are very similar to those observed in the temperature evolution sequence. The XRD patterns, Figs. 8(b)–(d), again display evidence for the transformation from the nanocrystalline rock-salt phase to the layered dinitride structure. As seen in Figs. 8(e)–(j), a morphological change similar to the one described above occurs in the particles as they transform from a spheroidal shape corresponding to the nanocrystalline rock-salt phase to the platelet shape representative of the layered phase. Again, as Figs. 8(i) and (j) show, a number of the platelets are well faceted and hexagonal in shape. The size of the nanocrystalline spheroids isolated at the 6 min treatment are approximately 5–10 nm in diameter. The platelets observed in the 5 h heat treated sample are typically 1–2 nm in thickness and 10–20 nm in width, whereas the platelets in the 70 h heat treated sample appear to have coarsened slightly and are approximately 1–3 nm thick and 10–30 nm wide. Again, chemical analysis of each of the powders using EDAX and PEELS demonstrated the expected ratio of metals and nitrogen, i.e., $\sim$1:1:2 for Cr:W:N.

Because of the nanocrystalline nature of the rock-salt phase, it was not possible by conventional TEM analysis to clearly establish an orientation relationship between the L-$CrWN_2$ and rock-salt structured compound out of which the layered phase nucleates and grows. However, it is possible to re-examine the HRTEM intergrowth micrographs reported by Svensson and Weil [7] in light of the new phase transformation data. The HRTEM analysis was conducted on a sample that had been heat treated at 750°C for 20 h in flowing ammonia gas. According to the graph in Fig. 6, approximately 2% of the disordered rock-salt phase would remain untransformed in this sample, a small enough fraction that it could not be detected by XRD. Shown in Fig. 9(a) is an example of a triple point region containing both phases. The region marked as A is a crystallite of $CrWN_2$ as viewed along a $\langle 2\bar{1}\bar{1}0 \rangle$ axis. Rotated counter-clockwise

Fig. 7. A series of isochronal experiments conducted at 650°C, 700°C, and 750°C for 5 h: (a) the corresponding relationship to the TTT curve, (b) the diffraction pattern of the Cr–W precursor heat treated in ammonia at 650°C for 5 h, (c) the diffraction pattern of the Cr–W precursor heat treated in ammonia at 700°C for 5 h, and (d) the diffraction pattern of the Cr–W precursor heat treated in ammonia at 750°C for 5 h. The circles denote the Bragg reflections for the rock-salt structured phase, while the asterisks represent the Bragg reflections for the layered phase. TEM micrographs from a series of isochronal experiments in which the Cr–W precursor was heat treated for 5 h in ammonia at: (e) 650°C (135 kx magnification), (f) 700°C (230 kx), (g) 750°C (230 kx), (h) 650°C (300 kx), (i) 700°C (300 kx), and (j) 750°C (380 kx).

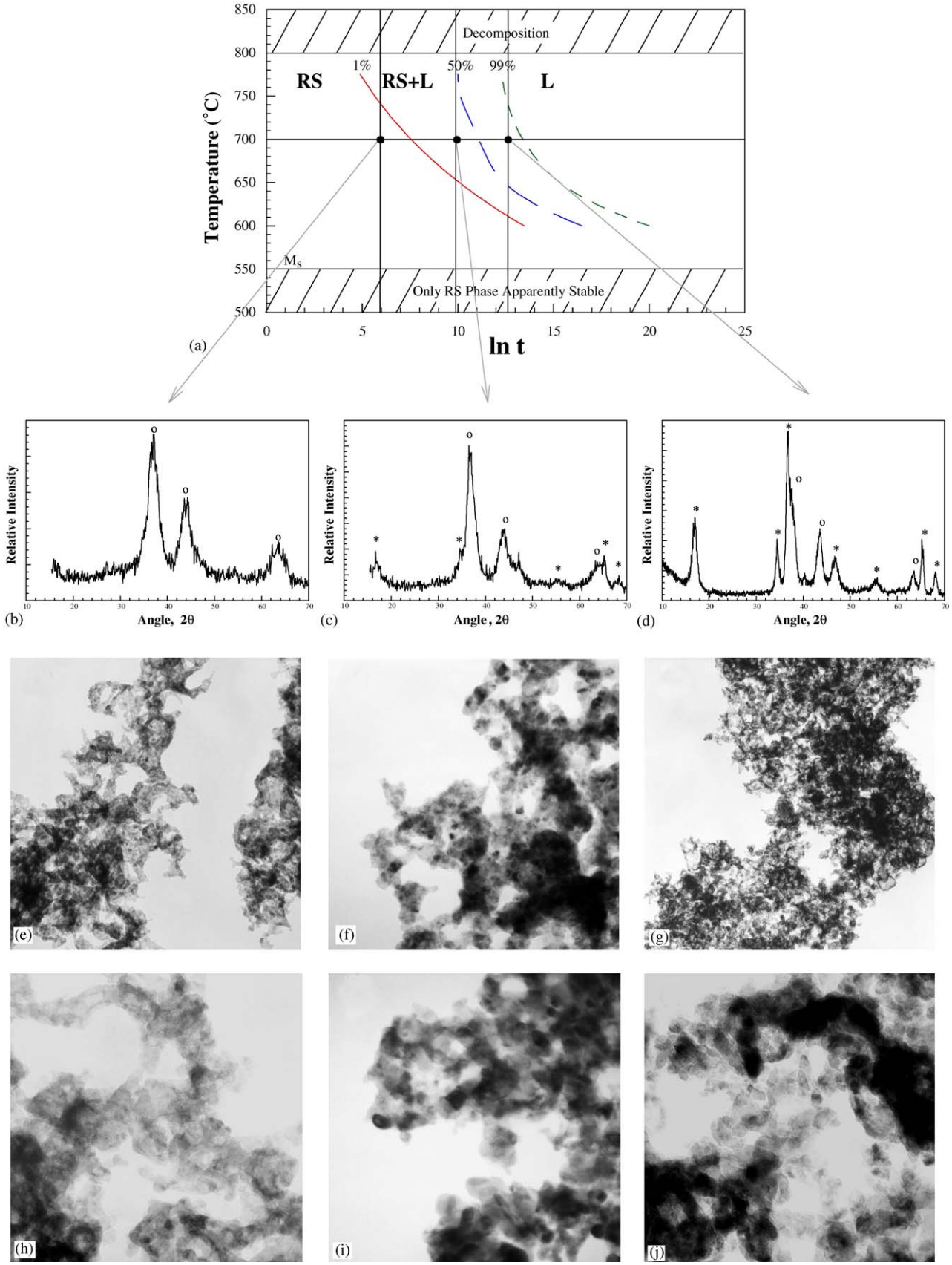
Temperature (°C)
ln t
Decomposition
RS
RS+L
L
1%
50%
99%
M_S
Only RS Phase Apparently Stable
(a)
Relative Intensity
Angle, 2θ
(b)
(c)
(d)
(e)
(f)
(g)
(h)
(i)
(j)

72° to the layers in A and also oriented along $\langle 2\bar{1}\bar{1}0 \rangle$, is a second fragment of $CrWN_2$ marked as B. Between the two $CrWN_2$ crystallites, at region C, is a phase which displays a rock-salt structured electron diffraction pattern. The structural model for this micrograph, based on the image contrast simulation of this micrograph is shown in Fig. 9(b). Both the micrograph and the structural model suggest an epitaxial relationship between the {111} planes of the disordered rock-salt phase and the {0001} basal planes of the layered phase. The strain introduced at the interface between the (111) plane of rs-$Cr_{0.5}W_{0.5}N$ and the (0001) plane of $CrWN_2$ is estimated to be 1.9% based on the average difference in atom-to-atom spacing in the corresponding crystallographic planes, which is small enough that the two planes remain epitaxial without the need for misfit dislocations to take up the geometric mismatch [21].

That an epitaxial relationship exists between the {111} planes of the rock-salt structured phase and the {0001} planes of the layered phase is not surprising. The equivalency of these planes is shown schematically in Fig. 10, which gives a direct structural comparison between the two phases and the relationship between their stacking arrangements. Both structures have a FCC-type stacking arrangement. In fact, the layered structure can be described as a derivative of the rock-salt structure in the same way that the rock-salt structure is described as a derivative of the simple FCC structure:

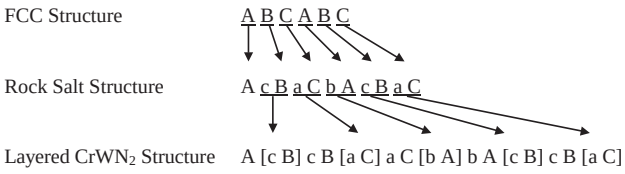

where the upper case letters denote closest-packed metal layers and the lower case letters denote the closest-packed nitrogen layers. That is, the rock-salt structure can be viewed as a simple FCC structure with a single closest-packed nitrogen layer placed in between the {111} metal layers and the layered $CrWN_2$ structure is the rock-salt structure with a pairing of a closest-packed nitrogen layer and the corresponding closest-packed metal layer placed in between the paired metal–nitrogen slabs.

This description of the slight structural differences between the rock-salt and layered nitrides correlates well with our experimentally determined values of activation energy, E_a, and the time exponent, n, for the phase transformation. As shown by the two- and three-dimensional schematics of the transforming interface between the two phases in Figs. 11(a) and (b), the diffusion distances for this order–disorder transformation are small. Thus the energy barrier, or activation energy, for this type of transformation is expected to be quite low, which agrees with our measured value of E_a. The value of the time exponent is dependent on the

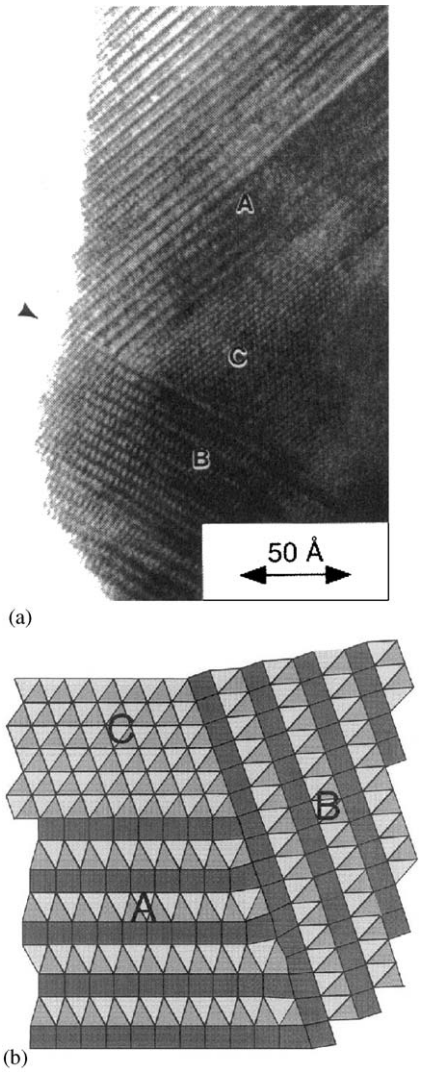

Fig. 9. (a) A triple point region in a chromium–tungsten powder heat treated in flowing ammonia at 750°C for 20 h. Regions A and B consist of $CrWN_2$ intergrown along $\{10\bar{1}2\}$ and {0001}, respectively. On the other hand, region C appears to be composed of cubic close packed type phase, presumed to be $Cr_{0.5}W_{0.5}N$. (b) A structural interpretation of the triple junction in (a).

Fig. 8. A series of isothermal experiments conducted at 700°C for 0.1, 5, and 70 h: (a) the corresponding relationship to the TTT curve, (b) the diffraction pattern of the Cr–W precursor heat treated in ammonia at 700°C for 0.1 h, (c) the diffraction pattern of the Cr–W precursor heat treated in ammonia at 700°C for 5 h, and (d) the diffraction pattern of the Cr–W precursor heat treated in ammonia at 700°C for 70 h. The circles denote the Bragg reflections for the rock-salt structured phase, while the asterisks represent the Bragg reflections for the layered phase. TEM micrographs from a series of isothermal experiments in which the Cr–W precursor was heat treated in ammonia at 700°C for: (e) 0.1 h (135 kx magnification), (f) 5 h (230 kx), (g) 70 h (135 kx), (h) 0.1 h (300 kx), (i) 5 h (300 kx), and (j) 70 h (380 kx).

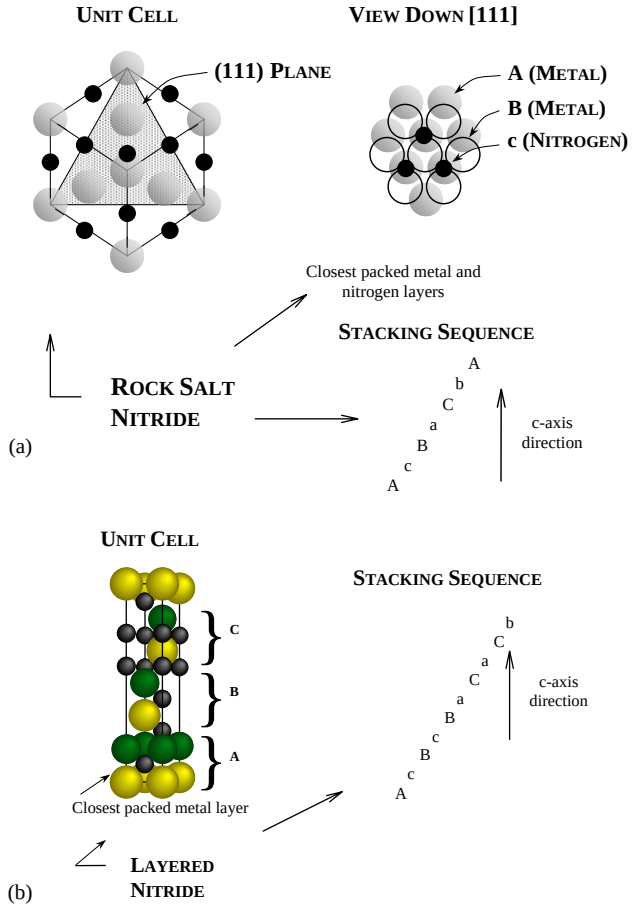

Fig. 10. A comparison of the unit cell structures and closest-packed layers in the (a) rock-salt, and (b) layered $CrWN_2$ structures. Note the similarities in the stacking arrangements.

conditions under which nucleation and growth take place and can be described using a simple empirical equation first suggested by Johnson and Mehl [15]:

$$n = p + q, \tag{3}$$

where p is the nucleation factor: $p = 0$ for immediate, burst-type nucleation (at transformation time, $t = 0$) and $p = 1$ for constant nucleation with time, and q is related to the geometry and dimensionality of the new growing phase. For platelet-shaped particles, $q = 1$ for two-dimensional growth, i.e., growth across the interface between the two phases [17]. Thus based on the value of n resulting from the analysis of our nucleation kinetics data, it is likely that $CrWN_2$ nucleates in a single burst event and grows epitaxially on $Cr_{0.5}W_{0.5}N$ via a two-dimensional order–disordered transformation mechanism, where cations move the distance of a cubic lattice spacing or so into ordered planes of the rhombohedral structure as the transformation front progresses from the rock-salt structured nitride into the layered compound.

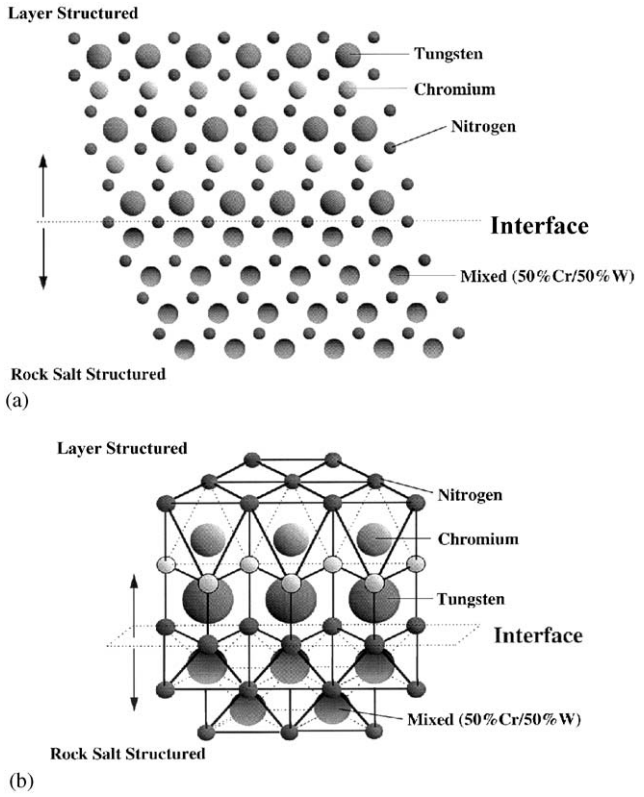

Fig. 11. (a) A two-dimensional schematic of the epitaxial interface between the growing layered phase and the rock-salt structured phase. A three-dimensional interpretation is shown in (b).

4. Conclusion

We have discovered a disorder–order phase transformation that occurs in the transition metal nitride containing a 1:1:2 ratio of Cr:W:N. Between ~550°C and 775°C, the rock-salt form of the nitride with random cation ordering transforms to the layered compound, $CrWN_2$. Kinetic analysis of the transformation indicates that it occurs epitaxially at the interface between the two phases via a two-dimensional growth mechanism. Because of the close structural similarities between the rock-salt and layered phases, the transformation is presumed to transpire over very small diffusion distances, requiring only a modest activation energy to take place.

Acknowledgments

The author gratefully acknowledges the assistance of Tom Nuhfer at Carnegie Mellon University and Professor Gunnar Svensson at Stockholm University in conducting the TEM and HRTEM analyses on $CrWN_2$. The author would also like to thank Professor David Laughlin at Carnegie Mellon University for his valuable suggestions in evaluating the phase

transformation data. The author also gratefully acknowledges the financial support of the International Center for Diffraction Data.

References

[1] D.H. Gregory, P.M. O'Meara, A.G. Gordon, D.J. Siddons, A.J. Blake, M.G. Barker, T.A. Hamor, P.P. Edwards, J. Alloys Compd. 317–318 (2001) 237.
[2] S. Yamanaka, K. Hotehama, H. Kawaji, Nature 392 (1998) 580.
[3] H. Jacobs, E. von Pinkowski, J. Less-Common Met. 146 (1989) 147.
[4] S.H. Elder, F.J. DiSalvo, L. Topor, A. Navrotsky, Chem. Mater. 5 (1993) 1545.
[5] R. Niewa, F.J. DiSalvo, Chem. Mater. 10 (1998) 2733.
[6] K.S. Weil, P.N. Kumta, J. Solid State Chem. 128 (1997) 2.
[7] G. Svensson, K.S. Weil, J. Mater. Chem. 9 (1999) 2709.
[8] K.S. Weil, Ph.D. Thesis, Carnegie Mellon University, 1999.
[9] W. Levason, C.A. McAuliffe, F.P. McCullough, Inorg. Chem. 16 (1977) 2911.
[10] B.L. Averbach, M. Cohen, Trans. AIME 176 (1948) 401.
[11] R.A. Young, D.B. Wiles, J. Appl. Crystallogr. 14 (1981) 149.
[12] J. Rodriguez-Carvajal, M.T. Fernandez-Diaz, J.L. Martinez, J. Phys: Condens. Matter 3 (1991) 3215.
[13] P. Thompson, D.E. Cox, J.B. Hastings, J. Appl. Crystallogr. 20 (1987) 79.
[14] ASTM D5373-93 Standard test methods for instrumental determination of carbon, hydrogen, and nitrogen in laboratory samples of coal and coke, 1997.
[15] W.A. Johnson, R.F. Mehl, Trans. AIME 135 (1939) 416.
[16] M. Avrami, J. Chem. Phys. 7 (1939) 1103.
[17] M.E. McHenry, M.A. Willard, D.E. Laughlin, Progr. Mater. Sci. 44 (1999) 291.
[18] F.W. Dynys, J.W. Halloran, J. Am. Ceram. Soc. 65 (1982) 442.
[19] E.J. Mittemeijer, L. Cheng, P.J. van der Schaff, C.M. Brakman, B.M. Korevaar, Met. Trans. 19A (1988) 925.
[20] L.J. Bowen, R.J. Weston, T.G. Carruthers, R.J. Brook, J. Mater. Sci. 13 (1978) 341.
[21] D. Hull, D.J. Bacon, Introduction to Dislocations, 3rd Edition, Pergamon Press, Oxford, 1984.